Volume 1 | Number 1 | Jan 2013 | Pages 1–100

Journal of
Materials Chemistry B

Materials for biology and medicine
www.rsc.org/materialsB

ROYAL SOCIETY
OF CHEMISTRY

ROYAL SOCIETY
OF CHEMISTRY

www.rsc.org/materialsB

ARTICLE TYPE

Three-dimensional Fe- and N-incorporated carbon structures as peroxidase mimics for fluorescent detection of hydrogen peroxide and glucose

Ruizhong Zhang, [a,b] **Shuijian He,**[a,b] **Chunmei Zhang**[a,b] **and Wei Chen**[*a]

In this study, a simple and one-pot pyrolysis strategy is developed to the mass production of Fe, N-incorporated carbon nanotubes *in situ* grown on 3D porous carbon foam (denoted as Fe-Phen-CFs), which provides highly active Fe-N and doped-N species, and large surface area with exposed active sites. The [10] obtained composite exhibits intrinsic peroxidase-like catalytic activities. With the Fe-Phen-CFs as catalyst, the peroxidase substrate of terephthalic acid (TA) can be oxidized to the fluorescent product of hydroxyterephthalate (HTA) by H_2O_2, which provides a unique strategy for fluorescent detection of H_2O_2. With such process, as low as 68 nM H_2O_2 could be detected with a linear range from 0.1 to 100 μM. Meanwhile, by integrating glucose oxidase on the Fe-Phen-CFs composite, sensitive detection of glucose [15] is also achieved with a linear range from 0.5 to 200 μM and a limit of detection of 0.19 μM. Most importantly, such novel TA/Fe-Phen-CFs system can be successfully applied to glucose determination in real human serum samples. The unique nature and 3D structure of Fe-Phen-CFs composite makes it promising for the fabrication of low-cost, high-performance biosensors.

[20] 1. Introduction

Hydrogen peroxide (H_2O_2) is not only of great importance in the fields of pharmaceutical, food science, chemistry, environmental protection and mining but also acts as an oxidative stress marker and a defense agent in response to pathogen [25] invasion in a physiological process.[1-3] In living organisms, H_2O_2 bursts can trigger several classes of essential signaling proteins that affect cell proliferation and thus lead to various diseases, including cancer, diabetes, cardiovascular and neurodegenerative disorders.[4-8] Therefore, the sensitive detection of H_2O_2 is one of [30] the most important research issues in chemical and biological fields. As another important compound, glucose is an energy source for the living cells and metabolic intermediate in biological systems. Much research has demonstrated that diabetes and some cancers are associated with the breakdown of glucose [35] transport in human body.[9-11] Therefore, one of the major challenges in the prevention of these diseases is sensitively monitoring glucose concentration. The glucose oxidase (GOD) can catalyze the oxidation of glucose to gluconolactone and H_2O_2[12]: glucose + O_2 → GOD → gluconolactone + H_2O_2. Thus, [40] the quantification of glucose can be achieved by indirect detection of the concentration of enzymatically liberated H_2O_2.

To date, various methods have been developed for detecting H_2O_2 and glucose, including colorimetry,[13-16] electrochemistry,[9, 17-23] chemiluminescence[24-26] and fluorescence detection.[27-30]

[45] Among these techniques, fluorometric approach has attracted special interest because of their highly sensitivity and specificity. In addtion, fluorometric tecnique usually does not need expensive or sophisticated instruments, complicated operation and detection procedures. So far, many glucose and H_2O_2 sensors heve been [50] fabricated; however, peroxidases have been frequently chosen to develop those sensors. The intrinsic drawbacks, such as instability, high cost and critical operating condition may limit their practical applications. Recently, nanomaterial-based peroxidase mimics have received considerable attention owing to [55] their advantages of low cost, tunable catalytic activity etc.[31-34] A variety of nanomaterials, including Au nanoclusters /nanoparticles,[24, 35, 36] Pt nanoparticles (NPs),[37] Au@Pt nanostructures,[38, 39] Fe_3O_4 NPs,[40, 41] Co_3O_4 NPs,[42] CuO (Cu_2O) NPs,[43-45] V_2O_5 nanowires,[46] carbon dots[47, 48] and single-walled [60] carbon nanotubes,[49] have already been employed as enzyme mimics. However, noble metal nanomaterials have high cost and tedious preparation procedures. Meanwhile, most of them are unstable and prone to be aggregated in aqueous solutions, leading to the decrease of specific surface area and catalytic activities.[50] [65] To solve these bottlenecks, organic ligands are introduced on particle surface to improve the stability and dispersion of nanomaterials. However, complicated surface modification is required and the presence of surface ligands might suppress the catalytic activity of nanomaterials.[36, 51]

[70] Recently, the emergence of composites fabricated by loading nanomaterials onto carbon matrices with large surface area, such

as graphene and carbon nanotubes, provides an alternative way to enhance the stability and dispersion of nanomaterials.[52-55] Typically, such composites usually exhibit enhanced catalytic activity and/or some novel properties compared with nanomaterials alone, due to the enlarged active surface area and the synergic effect of nanomaterial and the carbon matrix. In recent years, transition metal-nitrogen-carbon composites (M/N/C, M = Fe, Co) have been synthesized and studied extensively as low-cost and precious metal-free catalysts for oxygen reduction reaction in both acidic and alkaline fuel cells.[56-61] Although exact understanding on the nature of the active sites in these composites remains controversial, it has been extensively identified that a majority of such potential composites either possess doped nitrogen or metal-coordinated nitrogen species in the carbon matrix. To the best of our knowledge, there are no reports on the exploration of the catalytic property of M-N-C composites in fluorescent sensor,.

In the present study, Fe- and N- simultaneously incorporated carbon nanostructures (donated as Fe-Phen-CFs) were successfully prepared through a one-pot thermolysis of commercially available melamine foam impregnated with 1, 10-phenanthroline and iron complex. The obtained Fe-Phen-CFs composite showed intrinsic peroxidase-like catalytic activities. By taking advantage of the peroxidase-like catalytic activity of the Fe-Phen-CFs composite and using TA as a fluorescent peroxidase substrate, a TA/Fe-Phen-CFs system was fabricated for the determination of H_2O_2. In the presence of hydrogen peroxide, the Fe-Phen-CFs composite can effectively catalyze the decomposition of hydrogen peroxide into hydroxyl radicals followed by an oxidation reaction between the hydroxyl radical and terephthalic acid (TA), giving a remarkable fluorescent signal. On the other hand, H_2O_2 is a product of enzymatic reactions between GOD and glucose in the presence of oxygen, based on which a simple fluorescent method was also developed to detect glucose by integrating GOD and Fe-Phen-CFs composite. Under optimal conditions, as low as 68 nM H_2O_2 could be detected with a linear range from 0.1 to 100 μM, and 0.19 μM glucose can be determined with the linear range from 0.5 to 200 μM. In addition, the novel TA/Fe-Phen-CFs system was successfully applied to the glucose determination in real human serum samples.

2. Experimental Section

2.1 Materials

1, 10-phenanthroline ($C_{12}H_8N_2$, 99%) was purchased from Alfar Aesar. Iron (II) sulfate heptahydrate ($FeSO_4 \cdot 7H_2O$, A.R. grade, ≥99.0%), hydrogen peroxide (H_2O_2, A.R. grade, 30%) and glucose ($C_6H_{12}O_6 \cdot H_2O$, A.R. grade) were obtained from Beijing Chemical Works. Terephthalic acid ($C_8H_6O_4$, ≥99.0%) was purchased from Sinopharm Chemical Reagent Co., Ltd (Shanghai, China). Glucose oxidase was purchased from Aladdin Reagent Company (Shanghai, China). Melamine foam was supplied by Puyang Green Universh Chemical Co., Ltd. All chemicals were used as received without further purification. And all aqueous solutions were prepared with ultrapure water supplied by a Water Purifier system (18.3 MΩ cm).

2.2 Synthesis of Fe-Phen-CFs composite

The composites were synthesized through the following procedure by using iron (II) sulfate ($FeSO_4$), 1, 10-phenanthroline (Phen) and commercial melamine foam. Typically, $FeSO_4$ (0.0898 g) and Phen (0.1748 g) were first dissolved and mixed in 160 mL anhydrous ethanol in a vessel with a molar ratio of 1:3 to form a salmon Fe-Phen complex. Then 0.4610 g of melamine foam slices was soaked in the complex solution and the vessel was continuously shaken for 12 h at room temperature allowing the thorough absorption of Fe-Phen complex on melamine foam slices. The fully impregnated melamine foam slices were evaporated at 70 ^{o}C for 10 h to remove the solvent. Then, the ceramic boats containing the dried slices were placed in a tube furnace and heated at 800 ^{o}C in a nitrogen atmosphere for 1 h with a heating rate of 2 ^{o}C/min. The heat-treated material was then leached with 0.5 M H_2SO_4 to remove any metallic or metal oxide crystallites that might have formed during the thermolysis. The leached sample was heat-treated again at the same temperature under nitrogen atmosphere. The product was denoted as Fe-Phen-CFs.

For comparison, through the similar process, Fe-CFs was also synthesized without the addition of Phen, and carbonized melamine foams (CFs) was prepared by pyrolysing pure commercial melamine foam at 800 ^{o}C under nitrogen atmosphere.

2.3 Characterization

The morphologies of the as-prepared materials were characterized with a XL30 ESEMFEG scanning electron microscope (FE-SEM) operating at an accelerating voltage of 20 kV, and elemental analyses of the materials were carried out using techniques of energy dispersive X-ray spectroscopy (EDS), equipped in the FE-SEM. High-resolution transmission electron microscopy (HRTEM) images were collected on a JEM-2010 (HR) microscope operated at 200 kV. Powder X-ray diffraction (XRD) was performed on a D8 ADVANCE (Germany) using Cu Kα radiation with a Ni filter (λ = 0.154059 nm at 30 kV and 15 mA) to examine the crystallinity of the products. X-ray photoelectron spectroscopy (XPS) measurements were performed by using a VG Thermo ESCALAB 250 spectrometer (VG Scientific) operated at 120 W. The binding energy was calibrated against the carbon 1s line. Fluorescence spectra were obtained using a Fluoromax-4 spectrofluorometer (Horiba Jobin Yvon Inc.).

2.4 Hydrogen peroxide determination

In a typical hydrogen peroxide (H_2O_2) assay, an appropriate concentration of H_2O_2 (0.5 mL) was added to a brown vial containing of Fe-Phen-CFs (20 μg), TA (25 mM, 0.8 mL) and phosphate buffer (0.2 M, 3.65 mL, pH = 7.0). The mixture was incubated at 50 ^{o}C for 20 min. Then the fluorescence spectrum was collected on a Fluoromax-4 spectrofluorometer under the excitation wavelength of 315 nm.

2.5 Glucose detection

Different concentrations of glucose (0.5 mL), GOD (1 mg/mL, 62.5 μL) and phosphate buffer solution (0.2 M, 62.5 μL, pH = 7.0) were added into a brown vial and incubated at 37 ^{o}C for 20 min. Then phosphate buffer solution (0.2 M, 3.525 mL, pH = 7.0), Fe-Phen-CFs (20 μg), and TA (25 mM, 0.8 mL) were added to the above glucose reaction solution for another 2 h at 50 ^{o}C. The resulting reaction solution was measured by using a Fluoromax-4 spectrofluorometer under the excitation wavelength of 315 nm.

2.6 Serum samples detection

For glucose determination in serum, a serum sample was first pretreated by centrifugation at 7000 rpm for 15 min to eliminate the possible interference of proteins by using an Amicon Ultra
5 filter with a 3000 molecular weight cutoff. The obtained sample was diluted by a phosphate buffer solution and determined in the same way as the procedures mentioned above for glucose detection. The results of proposed method were compared with that of measured by the glucose oxidase endpoint method in
10 hospital.
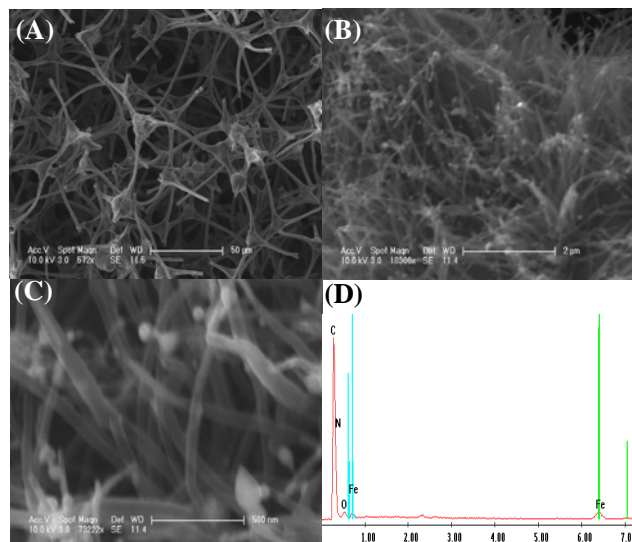
30 **Fig. 1** (A-C) SEM images of the 3D iron- and nitrogen-incorporated carbon structures (Fe-Phen-CFs) at different magnifications. (D) EDS pattern of the Fe-Phen-CFs.

3. Results and Discussion

3.1 Synthesis and characterization of 3D Fe-Phen-CFs
35 **composite**

By using a facile one-pot thermolysis strategy, iron- and nitrogen-incorporated 3D carbon nanostructure (Fe-Phen-CFs) was synthesized with commercially available melamine foam, iron salt ($FeSO_4$) and 1, 10-phenanthroline (Phen) as precursors. For
40 comparison, Fe-incorporated carbon composite without addition of Phen (Fe-CFs) and carbonized melamine foam (CFs) were also synthesized. The morphologies of the as-synthesized samples were first investigated by SEM. As can be seen from Fig. S1A and B, the CFs prepared by pyrolyzing pure melamine foam are
45 composed of branched fibers with a diameter of several micrometers and these branches entwine each other to form three-dimensional typical open-cell network structure. After the pyrolysis of melamine foam impregnated with the complex of iron (II) and Phen at 800 °C under N_2 atmosphere for one hour,
50 the obtained product (Fe-Phen-CFs) still maintained the intrinsically three-dimensional frame of carbon foams (Fig. 1A). From the magnified SEM images of Fe-Phen-CFs composite shown in Fig. 1B and C, the skeleton of carbon foams is covered by a closely packed layer of vertically stood carbon nanotubes,
55 which is quite different from the smooth surface of CFs (Fig. S1C). These SEM characterizations clearly show that carbon nanotubes have been successfully *in situ* grown on the surface of carbon foams. The corresponding energy dispersive X-ray

spectroscopy (EDS) (Fig. 1D) indicates that iron content has been
60 incorporated in the Fe-Phen-CFs composite except for the intrinsic nitrogen and carbon presented in carbon foam (Fig. S1D). However, in the absence of Phen during the pyrolysis process, no carbon nanotubes were formed on the surface of carbon foam, and only aggregated metal nanoparticles are distributed on the
65 skeleton of carbon foam, as shown in Fig. S2A-C. This result indicates coordinated metal may be favorable for the *in situ* growth of carbon nanotubes on the carbon foam under the present condition. Therefore, compared to the CFs and Fe-CFs, the Fe-Phen-CFs hybrid could provide enhanced surface area with
70 exposure of catalytically active sites, and large pore size for facile mass transportation.
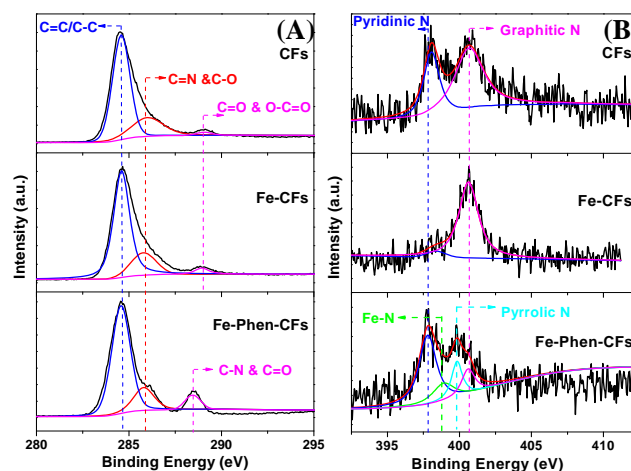
Fig. 2 High resolution XPS spectra of C1s (A) and N1s (B) for the three
90 samples of CFs, Fe-CFs and Fe-Phen-CFs.

X-ray photoelectron spectroscopy (XPS) measurements were performed to investigate the chemical composition and chemical states of C, N and Fe in the Fe-Phen-CFs composite. The XPS
95 survey spectrum in Fig. S3A distinctly shows the presence of four predominant peaks at 285.9, 400.3, 534.9 and 723.0 eV, corresponding to the binding energies of C_{1s}, N_{1s}, O_{1s} and Fe_{2p}, respectively. This result indicates that after pyrolyzing the melamine foam soaked with the complex of Fe (II) and Phen,
100 nitrogen and iron have been successfully incorporated into the carbon foam composite, in agreement with the EDS results. Based on the XPS spectra, the contents of C, N and Fe in the Fe-Phen-CFs composite were evaluated to be 96.71, 3.17 and 0.13%, respectively. In this work, melamine foam acts as a self-sacrificed
105 carbon and nitrogen precursor, and the introduction of Phen was expected to provide additional nitrogen source, which can be further confirmed by the C_{1s} XPS spectra. Fig. 2A compares the high-resolution C_{1s} spectra of CFs, Fe-CFs and Fe-Phen-CFs samples. From Fig. 2A an improved degree of nitrogen-doping in
110 Fe-Phen-CFs can be observed by the additional peak at 288.4 eV (C-N/C=O), in addition to the presence of peaks at 284.6 eV (C=C/C-C), 286.0 eV (C-O/C=N) and 289.1 eV (C=O/O-C=O) in all three samples.[62] The improved nitrogen-doping degree is believed to be an important contributing factor for the enhanced
115 catalytic activity of Fe-Phen-CFs. Moreover, the high-resolution N_{1s} XPS in Fig. 2B shows that the contents of pyridinic N

(398.35 eV) and graphitic N (400.8 eV) almost keep constant for the CFs, Fe-CFs and Fe-Phen-CFs samples, while those of the two peaks corresponding to Fe-N (398.9 eV) and pyrrolic N (399.9 eV) are significantly enhanced for the Fe-Phen-CFs composite. Therefore, it can be proposed that the pyrrolic N and Fe-N in Fe-Phen-CFs may contribute to the higher catalytic activity of Fe-Phen-CFs composite compared to other two carbon structures

Fig. S3B shows the X-ray diffraction (XRD) pattern of the as-prepared Fe-Phen-CFs composite. There are only two obvious diffraction peaks with 2θ centered at 26.0° and 43.2°, which can be indexed to the (002) and (100) planes of graphite structure. No information of crystalline iron or iron oxide phase indicates that the iron element in the composite exists as coordinated state, but not as nanocrystal phase, which is consistent with the XPS results.
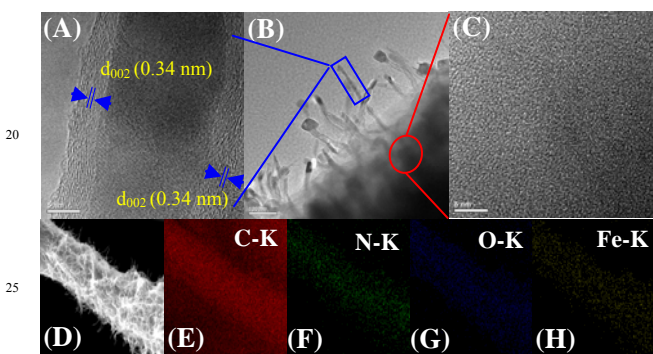
Fig. 3 (A-C) HRTEM micrographs of the Fe-Phen-CFs composite at different magnifications. Scale bars: (A) 5 nm; (B) 100 nm and (C) 5 nm. (D) Scanning electron microscopy image of the Fe-Phen-CFs and the corresponding elemental mapping of (E) C, (F) N, (G) O, and (H) Fe.

The morphology and crystal structure of the Fe-Phen-CFs composite were further examined by HRTEM. Fig. 3 A-C exhibit the HRTEM images of the 3D Fe-Phen-CFs composite at different magnifications. Clearly, the formed carbon nanotubes are vertically and firmly anchored on the surface of the carbon foam skeleton (Fig. 3B). The magnified image shown in Fig. 3A reveals the tubulate structure of the 1D carbon materials and presents the well-resolved lattice fringes with an interplanar spacing of 0.34 nm, referred to the (002) plane of graphite carbon. Such crystal structure clearly indicates the formation of multi-walled carbon nanotubes. On the other hand, from the magnified HRTEM image in Fig. 3C, the carbon foam skeleton substrate shows disorder carbon phase. The HRTEM images demonstrate again that multi-walled carbon nanotubes can be *in situ* formed on the skeleton of carbon foam after the pyrolysis of melamine foam impregnated with Fe(II)-Phen complex. During the pyrolysis, with the presence of transition metal (Fe), the disordered carbon phase of melamine foam can be partly transferred into a graphite carbon structure (carbon nanotubes) at a relatively low temperature (800 °C) under the catalysis of Fe. Moreover, Fe species can interact with amorphous carbon, and thus lead to the surface rearrangement by coordinating with nitrogen and carbon within the micropores.[63, 64] To gain further insight into the element distribution of the 3D Fe-Phen-CFs

nanostructure, scanning electron microscopy images and the corresponding elemental mapping were collected. From the elemental maps in Fig. 3E-H, it can be seen that four different elements of C, N, O and Fe are present in the 3D Fe-Phen-CFs composite, which is consistent with the XPS results. Fig. 3 F and H show that N and Fe are evenly distributed throughout the whole 3D composite. It could be proposed that with the growth of carbon nanotubes under the catalysis of Fe, Fe was not only doped in the carbon nanotubes but also detained within the micropores of carbon foam skeleton by forming the Fe-N bonds. These results indicate that melamine foam can serve as a promising carbon and nitrogen precursor for the growth of nitrogen-doped carbon nanotubes.
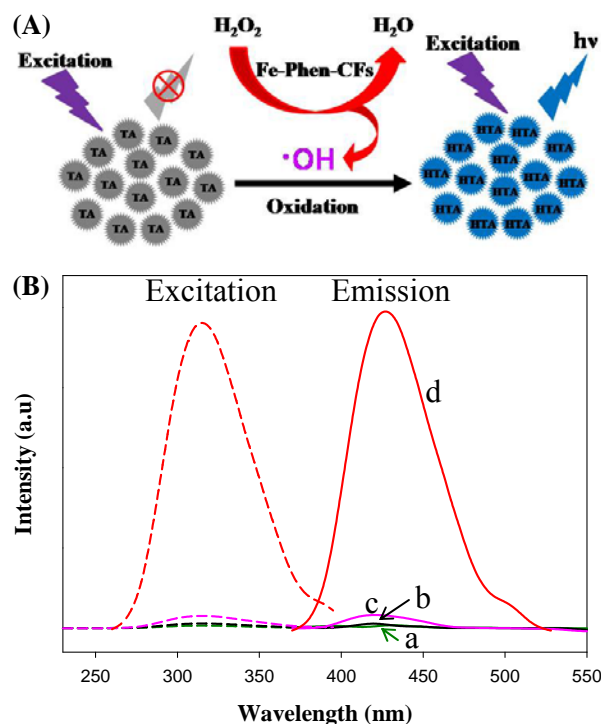
Fig. 4 (A) Schematic illustration of the Fe-Phen-CFs composite-based fluorescent sensor for H_2O_2 detection. (B)The excitation and emission spectra of TA (a), TA +Fe-Phen-CFs (b), TA+H_2O_2 (c) and TA+H_2O_2+Fe-Phen-CFs (d)

3.2 Peroxidase-like activity of Fe-Phen-CFs composite for H_2O_2 detection

The analytical determination of hydrogen peroxide is of great importance for medical diagnosis since hydrogen peroxide is an intermediate product formed in the case of various detection processes. Due to the highly active Fe-N specie together with doped-N species, and sufficient surface area of carbon nanotubes grown on the porous carbon foam, the Fe-Phen-CFs composite is expected to exhibit highly catalytic activity as a peroxidase mimetic for the fluorescent detection of hydrogen peroxide and glucose. The detection mechanism is shown in Fig. 4A. The original TA doesn't have fluorescence under excitation. In the

Journal Name

Dynamic Article Links ▶

ARTICLE TYPE
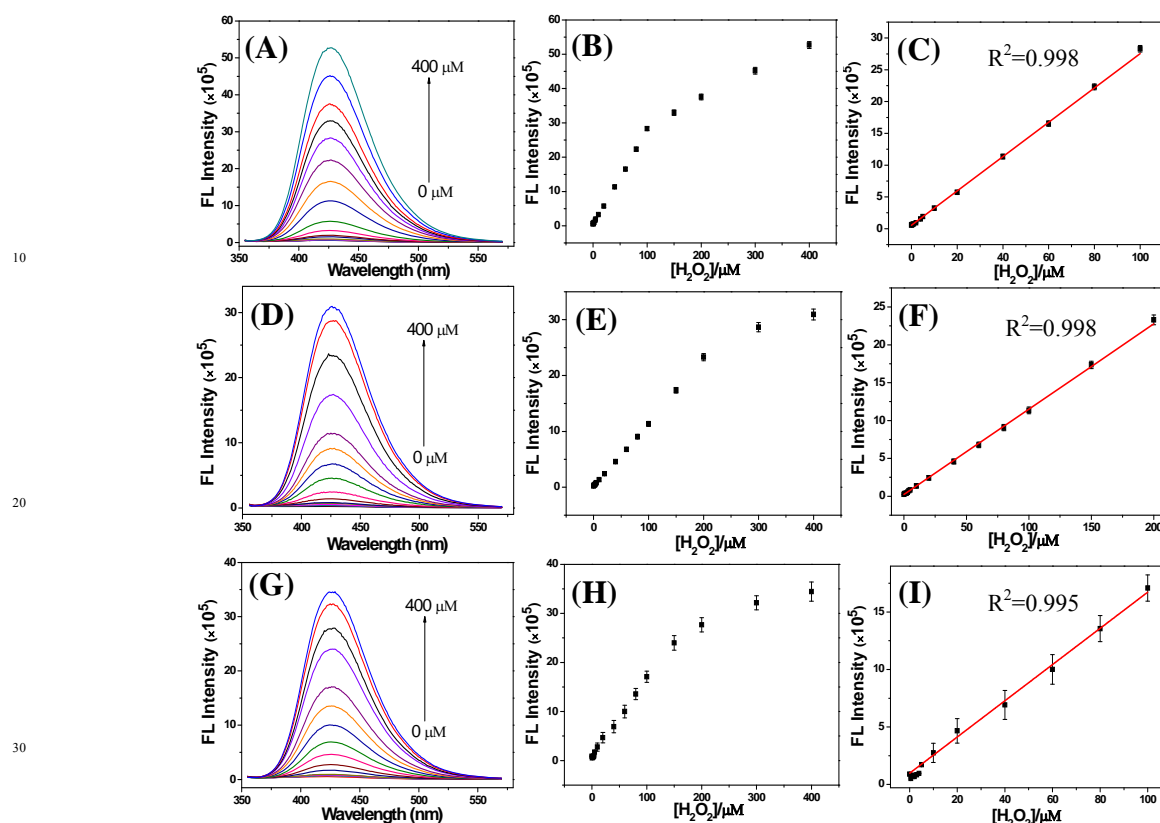
Fig. 5 Fluorescence responses to different concentrations of hydrogen peroxide (from 0 to 400 μM) in the TA (25 mM, 0.8 mL) and phosphate buffer (pH=7.0) solution with the presence of different catalysts: Fe-Phen-CFs (A), Fe-CFs (D) and CFs (G). (B, E, H) The corresponding dependence of fluorescence intensity on the hydrogen peroxide concentration with the three kinds of catalysts: Fe-Phen-CFs (B), Fe-CFs (E) and CFs (H). C, F and I show the calibration curves for the detection of hydrogen peroxide. All emission spectra were collected at λ_{ex} = 315 nm and at 50 °C

presence of hydrogen peroxide, a peroxidase mimetic of Fe-Phen-CFs can catalyze the break of O-O bonds to form hydroxyl radicals.[44, 65] An oxidation reaction then occurs between hydroxyl radical and TA to form hydroxyterephthalate (HTA) which can give fluorescence under a certain excitation. The detection of H_2O_2 could be achieved by using the dependence of fluorescence intensity on the concentration of H_2O_2. From Fig. 4B, it can be observed that HTA exhibits maximum emission at 426 nm when excited at 315 nm (curve d); however, no fluorescence is produced from TA (curve a) and TA/Fe-Phen-CFs (curve b). Although slow oxidation of TA can be induced by H_2O_2 without catalyst (curve c), the fluorescence is very weak. It can be seen that the fluorescence intensity could be greatly enhanced up to 30 folds with the presence of Fe-Phen-CFs catalyst. In addition, the fluorescence intensity of HTA was found to be proportional to the concentration of hydrogen peroxide. Thus by monitoring the fluorescence intensity, hydrogen peroxide can be detected sensitively. Compared to the traditional protein-based peroxidases, the present Fe-Phen-CFs composite is cost-efficient and highly stable.

In order to achieve the optimum assay performance, the experimental conditions, including solution pH, reaction temperature, TA concentration and the dose of Fe-Phen-CFs were optimized. The solution pH is an important factor that affects the catalytic activity of Fe-Phen-CFs in the sensing system. The experimental results are shown in Fig. S4A. With pH increasing, the fluorescence intensity firstly increases and then decreases rapidly, showing the maximum fluorescence intensity at pH = 7. Therefore, in the following fluorescence measurements, phosphate buffer (pH = 7.0) was used. The effect of TA concentration on the fluorescence intensity was also investigated. It can be seen from Fig. S4B that the fluorescence intensity increases with TA concentration increasing, and then keeps almost constant when the TA concentration is larger than 3.5 mM. Since excessive TA (non-fluorescent molecular) could not affect the fluorescence intensity of HTA, and in order to extend the linear range for the determination of hydrogen peroxide, 4 mM of TA was adopted in the following detection experiments. As shown in Fig. S4C, with the used amount of Fe-Phen-CFs increasing, the fluorescence intensity increases rapidly and then

reaches a constant value when the dosage is larger than 20 μg. Therefore, the optimal dosage of 20 μg of Fe-Phen-CFs catalyst was used for the subsequent analysis. Finally, the effect of reaction temperature on the fluorescence intensity was studied in the range of 25-60 °C, as shown in Fig. S4D. The fluorescence intensity of the sensing system increases with the increase of reaction temperature in the range of 25-50 °C and then decreases when temperature is higher than 50 °C. Based on this result, 50 °C was used as working temperature.

Under the optimal conditions described above, the TA oxidation reaction catalyzed by the Fe-Phen-CFs in the presence of hydrogen peroxide was then studied. The sensitivity of the proposed strategy towards hydrogen peroxide detection was investigated by adding a series of different concentrations of hydrogen peroxide into the catalytic system. Fig. 5A displays the change of emission spectra in response to the variation of hydrogen peroxide concentration in the range from 0 to 400 μM. As plotted in Fig. 5B, with hydrogen peroxide concentration increasing, an obvious increase of fluorescence intensity can be observed, demonstrating a concentration-dependent fluorescence response. Fig. 5C shows the calibration curve for quantitative analysis of hydrogen peroxide. The fluorescent intensity is linearly dependent on hydrogen peroxide concentration in the range from 0.1 to 100 μM. The calibration equation can be described as $I = 2.72 \times 10^4 [H_2O_2] + 6.16 \times 10^4$ (I is the fluorescence intensity at 426 nm, and $[H_2O_2]$ refers to the concentration of H_2O_2), and the calibration coefficient is $R^2 = 0.998$. The limit of detection (LOD) was estimated to be 68 nM based on three times the standard deviation rule (LOD=3SD/S). As shown in Table S1, the detection performance based on the present 3D Fe-Phen-CFs sensing material is superior to those of many previously reported fluorescent assay techniques.

Subsequently, the sensing properties of the as-prepared Fe-CFs and CFs catalysts for hydrogen peroxide detection were compared. Fig. 5D and G shows the fluorescence spectra obtained from Fe-CFs and CFs, respectively, with different concentrations of hydrogen peroxide. By comparing the spectra in Fig. 5A, D and G, it can be seen that at a same concentration of H_2O_2, the fluorescence intensity obtained from the Fe-Phen-CFs is much stronger than those from Fe-CFs and CFs, indicating the higher catalytic activity of the Fe-Phen-CFs structure. From Fig. 5E and H, the fluorescence intensities also show gradual increases with increasing the concentration of hydrogen peroxide, indicating both Fe-CFs and CFs could catalyze the oxidation of TA molecules to generate fluorescent HTA in the presence of hydrogen peroxide. As shown in Fig. 5F and I, Fe-CFs shows a linear range between 0.5 and 200 μM with LOD of 0.22 μM and CFs shows a linear response in the range from 0.5 to 100 μM with LOD of 0.32 μM for H_2O_2 detection. It is worth noting that the much higher sensitivity and lower LOD of Fe-Phen-CFs than those of Fe-CFs and CFs suggests the enhanced catalytic efficiency of Fe-Phen-CFs. The improved catalytic performance might be attributed to the additional and highly active pyrrolic N and Fe-N sites for catalyzing the break of hydrogen peroxide, as well as the unique morphology of the in situ formed carbon nanotubes with large surface area.

3.3 Glucose detection based on the 3D Fe-Phen-CFs structure

Reliable and fast detection of glucose is of considerable importance in clinical diagnostics and laboratory. Hydrogen peroxide is a product of glucose oxidase (GOD)-catalyzed enzymatic reactions of glucose in the presence of oxygen. Therefore, a simple fluorescent method was developed for the detection of glucose by integrating GOD and TA/Fe-Phen-CFs. In the presence of glucose and GOD, the product of the enzymatic reaction can be catalyzed by Fe-Phen-CFs to form hydroxyl radical. An oxidation reaction then occurs between hydroxyl radical and TA to form fluorescent HTA. As a result, glucose can be indirectly determined by monitoring the fluorescent intensity.
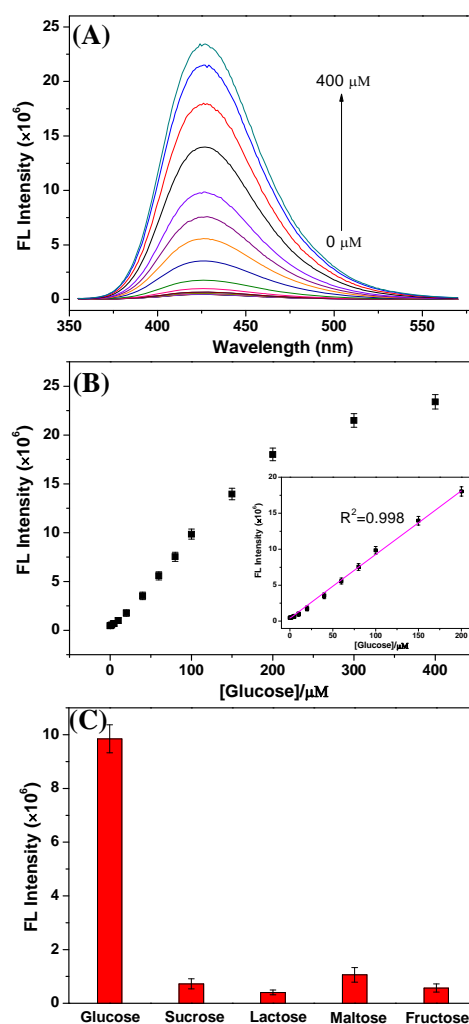
Fig. 6 (A) Fluorescent emission spectra of reaction solution in the presence of Fe-Phen-CFs upon addition of different concentrations of glucose ranging from 0 to 400 μM. (B) The dependence of fluorescence intensity on the glucose concentration. The inset shows the calibration curve between the fluorescence intensity and glucose concentration from 0.5 to 200 μM. (C) Fluorescence responses to glucose and various interferents. The concentrations of the studied species are as follows: sucrose, 500 μM; lactose, 500 μM; maltose, 500 μM; fructose, 500 μM; glucose 100 μM. All emission spectra were collected at λ_{ex} = 315 nm.

Based on above sensing mechanism and optimal conditions, the glucose detection based on Fe-Phen-CFs was investigated by adding different concentrations of glucose into the catalytic system. As shown in Fig. 6A, the fluorescence intensity at around

426 nm increases gradually with glucose concentration increasing, indicating that TA can be efficiently oxidized to fluorescent HTA molecules by the Fe-Phen-CFs. Fig. 6B presents the variation of fluorescence intensity versus the concentration of glucose. A good linear correlation (Fig. 6B inset, $R^2 = 0.998$) was obtained within the concentration range from 0.5 to 200 µM. The linear regression equation is as follows: $I = 8.97 \times 10^4$ [Glucose] $+ 3.21 \times 10^5$ (I is the fluorescence intensity at 426 nm and [Glucose] refers to the concentration of glucose). The detection limit was estimated to be 0.19 µM which is superior to those of many reported results (Table S2).

Furthermore, the detection selectivity of the proposed technique was evaluated by using glucose analogues, including sucrose, lactose, maltose and fructose, as interfering species. As can be seen from Fig. 6C, although the concentrations of interfering molecules are five-fold higher than that of glucose, very weak fluorescent signals were observed from the interferents due to the high substrate specificity of GOD. However, the sensing system shows strong fluorescence upon the addition of glucose. Such result demonstrates that the glucose sensor based on Fe-Phen-CFs structure has high selectivity for possible practical applications.
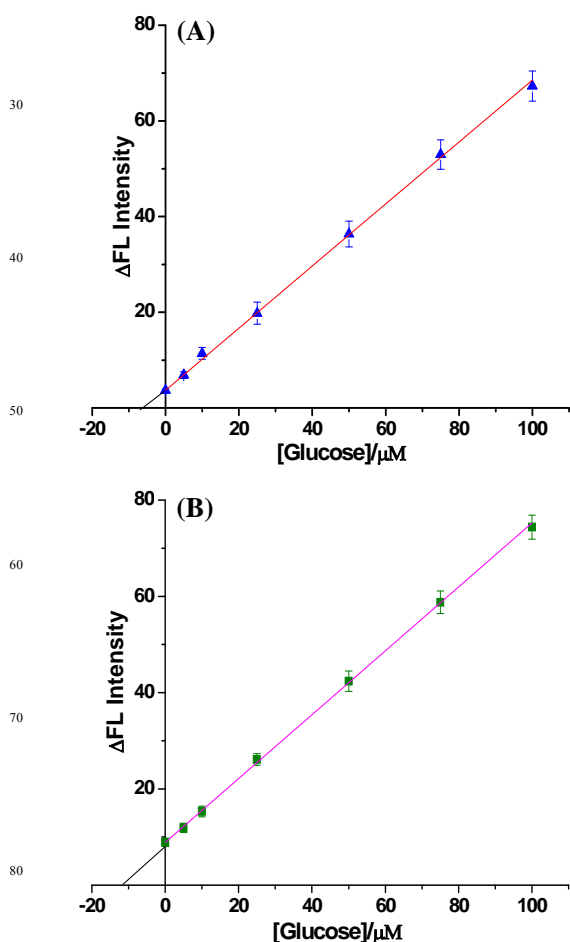
Fig. 7 Quantification of glucose concentrations in human serum sample 1 (A) and sample 2 (B) via the standard addition method.

3.4 Glucose determination in human serum

To evaluate the feasibility of the present sensing system for analysis of glucose in biological samples, the proposed method was applied to the detection of glucose in human serum samples. Serum samples were provided from Northeast Normal University Hospital. The serum samples were diluted 1000-fold before the analysis. The concentration of glucose in the human serum samples was quantified by using the standard addition method. In experiments, the even aliquots of human serum were added to standard solutions containing different concentrations of glucose from 0 to 100 µM and the resulting fluorescence was measured. The experimental data were plotted as the concentration of added standard glucose versus the obtained fluorescence intensity. As shown in Fig.7A and B, linear regressions were performed to get the X-intercept of the calibration lines, which correspond to the concentrations of glucose in the diluted real serum samples. Taking the dilution factor into consideration, the glucose concentrations of 5.75 and 13.37 mM in serum sample 1 and sample 2 were determined, respectively. As shown in Table 1, the results obtained from the proposed method are in good agreement with those measured by the glucose oxidase endpoint method in hospital. These results indicate the present TA/Fe-Phen-CFs-based fluorescent sensor may be a promising platform for the glucose analysis of real samples.

Table 1 Comparison of the analytical results of glucose sensing in human serum based on the present method and the glucose oxidase endpoint method in hospital

Samples	Proposed method (mM)	Hospital (mM)	Relative deviation (%)
Serum 1	5.75	5.90	2.54
Serum 2	13.37	13.10	2.06

4. Conclusion

In this work, we present a simple one-pot pyrolysis method for preparing Fe- and N-incorporated carbon nanotubes in situ grown on 3D porous carbon foam (denoted as Fe-phen-CFs). The obtained 3D composite could provide highly active Fe-N and doped-N species and large surface area with exposed catalytically active sites. The unique structure endows the Fe-Phen-CFs composite with intrinsic peroxidase-like activity and provides a fluorescent assay for hydrogen peroxide and glucose. The fluorescence sensing system based on TA/Fe-Phen-CFs showed a good response toward hydrogen peroxide with a linear range from 0.1 to 100 µM and a limit of detection of 68 nM. Moreover, by integrating GOD and Fe-Phen-CFs composite, sensitive assay of glucose was also obtained with the linear range from 0.5 to 200 µM and a limit of detection of 0.19 µM. In addition, such novel TA/Fe-Phen-CFs system was successfully applied to the glucose determination in real human serum samples. Compared to the traditional protein-based peroxidases, the Fe-Phen-CFs composite is cost-efficient and highly stable. We hope that the present study could promote the understanding of catalytic behaviors of Fe, N-functionalized carbon composites as enzyme mimics and develop their wide applications in biosensors.

Acknowledgements

5 ## Notes and references

a State Key Laboratory of Electroanalytical Chemistry, Changchun Institute of Applied Chemistry, Chinese Academy of Sciences, Changchun 130022, Jilin, China. Tel: +86431-85262723; E-mail: weichen@ciac.ac.cn

10 *b University of Chinese Academy of Sciences, Beijing 100039, China*
† Electronic Supplementary Information (ESI) available: More structural characterizations and comparison of the sensing performances of the present materials with those of the previously reported materials. See DOI: 10.1039/b000000x/

15

1 M. A. H. Alamiry, A. Harriman, L. J. Mallon, G. Ulrich and R. Ziessel, *Eur. J. Org. Chem.*, 2008, 2774-2782.

2. A. R. Lippert, G. C. V. De Bittner and C. J. Chang, *Acc. Chem. Res.*, 2011, **44**, 793-804.

20 3. Y. Y. Jiang, Y. Z. Lu, W. T. Wei, H.B. Wu, M.M. Liu, L. Niu,W. Chen, *J. Mater. Chem.*, 2012, **22**, 2929–2934.

4. E. W. Miller, B. C. Dickinson and C. J. Chang, *Proc. Nat. Acad. Sci. U.S.A.*, 2010, **107**, 15681-15686.

5. C. E. Paulsen and K. S. Carroll, *ACS Chem. Biol.*, 2010, **5**, 47-62.

25 6. C. C. Winterbourn, *Nat. Chem. Biol.*, 2008, **4**, 278-286.

7. S. G. Rhee, *Science*, 2006, **312**, 1882-1883.

8. S. G. Rhee, *Exp. Mol. Med.*, 1999, **31**, 53-59.

9. J. Zhao, L. M. Wei, C. H. Peng, Y. J. Su, Z. Yang, L. Y. Zhang, H. Wei and Y. F. Zhang, *Biosens. Bioelectron.*, 2013, **47**, 86-91.

30 10. J. Wang, *Chem. Rev.*, 2008, **108**, 814-825.

11. Z. G. Zhu, L. Garcia-Gancedo, A. J. Flewitt, H. Q. Xie, F. Moussy and W. I. Milne, *Sensors*, 2012, **12**, 5996-6022.

12. S. H. Lim, J. Wei, J. Y. Lin, Q. T. Li and J. KuaYou, *Biosens. Bioelectron.*, 2005, **20**, 2341-2346.

35 13. C. Radhakumary and K. Sreenivasan, *Anal. Chem.*, 2011, **83**, 2829-2833.

14. Y. Jiang, H. Zhao, Y. Q. Lin, N. N. Zhu, Y. R. Ma and L. Q. Mao, *Angew. Chem. Int. Ed.*, 2010, **49**, 4800-4804.

15. B. C. Zhu, H. L. Jiang, B. P. Guo, C. X. Shao, H. F. Wu, B. Du and Q.
40 Wei, *Sensor. Actuat. B-Chem.*, 2013, **186**, 681-686.

16. Y. J. Chen, H. Y. Cao, W. B. Shi, H. Liu and Y. M. Huang, *Chem. Commun.*, 2013, **49**, 5013-5015.

17. Y. F. Zhang, X. J. Bo, A. Nsabimana, C. Luhana, G. Wang, H. Wang, M. Li and L. P. Guo, *Biosens. Bioelectron.*, 2014, **53**, 250-256.

45 18. C. C. Kuo, W. J. Lan and C. H. Chen, *Nanoscale*, 2014, **6**, 334-341.

19. X. H. Niu, M. B. Lan, H. L. Zhao and C. Chen, *Anal. Chem.*, 2013, **85**, 3561-3569.

20. A. Xu, S. J. Jiang, Z. Hu and S. Q. Liu, *ACS Nano*, 2010, **4**, 4292-4298.

50 21. M. M. Liu, W. T. Wei, Y. Z. Lu, H. B. Wu and W. Chen, *Chinese J. Anal. Chem.*, 2012, **40**, 1477-1481.

22. J. Ju and W. Chen, *Anal. Chem.*, 2015, **87**, 1903-1910.

23. S. J. He, B. Y. Zhang, M. M. Liu and W. Chen, *RSC Adv.*, 2014, **4**, 49315-49323.

55 24. M. Deng, S. J. Xu and F. N. Chen, *Anal. Methods*, 2014, **6**, 3117-3123.

25. X. M. Li, L. Sun, A. Q. Ge and Y. S. Guo, *Chem. Commun.*, 2011, **47**, 947-949.

26. L. Hong, A. L. Liu, G. W. Li, W. Chen and X. H. Lin, *Biosens. Bioelectron.*, 2013, **43**, 1-5.

60 27. L. Zhang, Z. Y. Zhang, R. P. Liang, Y. H. Li and J. D. Qiu, *Anal. Chem.*, 2014, **86**, 4423-4430.

28. J. Xu, Q. Li, Y. Yue, Y. Guo and S. J. Shao, *Biosens. Bioelectron.*, 2014, **56**, 58-63.

29. P. F. Shen and Y. S. Xia, *Anal. Chem.*, 2014, **86**, 5323-5329.

65 30. F. Hu, Y. Y. Huang, G. X. Zhang, R. Zhao and D. Q. Zhang, *Tetrahedron Lett.*, 2014, **55**, 1471-1474.

31. Y. H. Lin, J. S. Ren and X. G. Qu, *Acc. Chem. Res.*, 2014, **47**, 1097-1105.

32. H. Wei and E. K. Wang, *Chem. Soc. Rev.*, 2013, **42**, 6060-6093.

70 33. Y. J. Guo, L. Deng, J. Li, S. J. Guo, E. K. Wang and S. J. Dong, *ACS Nano*, 2011, **5**, 1282-1290.

34. K. L. Fan, C. Q. Cao, Y. X. Pan, D. Lu, D. L. Yang, J. Feng, L. N. Song, M. M. Liang and X. Y. Yan, *Nat. Nanotechnol.*, 2012, **7**, 459-464.

75 35. Y. Jv, B. X. Li and R. Cao, *Chem. Commun.*, 2010, **46**, 8017-8019.

36. S. Wang, W. Chen, A. L. Liu, L. Hong, H. H. Deng and X. H. Lin, *Chemphyschem*, 2012, **13**, 1199-1204.

37. L. N. Zhang, H. H. Deng, F. L. Lin, X. W. Xu, S. H. Weng, A. L. Liu, X. H. Lin, X. H. Xia and W. Chen, *Anal. Chem.*, 2014, **86**, 2711-2718.

80 38. W. W. He, Y. Liu, J. S. Yuan, J. J. Yin, X. C. Wu, X. N. Hu, K. Zhang, J. B. Liu, C. Y. Chen, Y. L. Ji and Y. T. Guo, *Biomaterials*, 2011, **32**, 1139-1147.

39. J. B. Liu, X. N. Hu, S. Hou, T. Wen, W. Q. Liu, X. Zhu, J. J. Yin and X. C. Wu, *Sensor. Actuat. B-Chem.*, 2012, **166**, 708-714.

85 40. L. Z. Gao, J. Zhuang, L. Nie, J. B. Zhang, Y. Zhang, N. Gu, T. H. Wang, J. Feng, D. L. Yang, S. Perrett and X. Yan, *Nat. Nanotechnol.*, 2007, **2**, 577-583.

41. H. Wei and E. Wang, *Anal. Chem.*, 2008, **80**, 2250-2254.

42. J. S. Mu, Y. Wang, M. Zhao and L. Zhang, *Chem. Commun.*, 2012, **48**,
90 2540-2542.

43. W. Chen, J. Chen, Y. B. Feng, L. Hong, Q. Y. Chen, L. F. Wu, X. H. Lin and X. H. Xia, *Analyst*, 2012, **137**, 1706-1712.

44. A. L. Hu, Y. H. Liu, H. H. Deng, G. L. Hong, A. L. Liu, X. H. Lin, X. H. Xia and W. Chen, *Biosens. Bioelectron.*, 2014, **61**, 374-378.

95 45. M. M. Liu, R. Liu and W. Chen, *Biosens. Bioelectron.*, 2013, **45**, 206-212.

46. R. Andre, F. Natalio, M. Humanes, J. Leppin, K. Heinze, R. Wever, H. C. Schroder, W. E. G. Muller and W. Tremel, *Adv. Funct. Mater.*, 2011, **21**, 501-509.

100 47. W. B. Shi, Q. L. Wang, Y. J. Long, Z. L. Cheng, S. H. Chen, H. Z. Zheng and Y. M. Huang, *Chem. Commun.*, 2011, **47**, 6695-6697.

48. W. F. Zhu, J. Zhang, Z. C. Jiang, W. W. Wang and X. H. Liu, *RSC Adv.*, 2014, **4**, 17387-17392.

49. Y. J. Song, X. H. Wang, C. Zhao, K. G. Qu, J. S. Ren and X. G. Qu,
105 *Chem.-Eur. J.*, 2010, **16**, 3617-3621.

50. J. X. Xie, H. Y. Cao, H. Jiang, Y. J. Chen, W. B. Shi, H. Z. Zheng and Y. M. Huang, *Anal. Chim. Acta* 2013, **796**, 92-100.

51. A. Asati, S. Santra, C. Kaittanis, S. Nath and J. M. Perez, *Angew. Chem. Int. Ed.*, 2009, **48**, 2308-2312.

110 52. Y. L. Dong, H. G. Zhang, Z. U. Rahman, L. Su, X. J. Chen, J. Hu and X. G. Chen, *Nanoscale*, 2012, **4**, 3969-3976.

53. Y. Tao, Y. H. Lin, Z. Z. Huang, J. S. Ren and X. G. Qu, *Adv. Mater.*, 2013, **25**, 2594-2599.

54. W. B. Lu, X. Y. Qin, A. M. Asiri, A. O. Al-Youbi and X. P. Sun,
115 *Analyst*, 2013, **138**, 429-433.

55. J. Wang, K. Wang, F. B. Wang and X. H. Xia, *Nat. Commun.*, 2014, **5**, 5285.

56. Z. H. Xiang, Y. H. Xue, D. P. Cao, L. Huang, J. F. Chen and L. M. Dai, *Angew. Chem. Int. Edit.*, 2014, **53**, 2433-2437.

120 57. G. Nam, J. Park, S. T. Kim, D. B. Shin, N. Park, Y. Kim, J. S. Lee and J. Cho, *Nano Lett.*, 2014, **14**, 1870-1876.

58. J. Liang, R. F. Zhou, X. M. Chen, Y. H. Tang and S. Z. Qiao, *Adv. Mater.*, 2014, **26**, 6074-6079.

59. B. Zheng, J. Wang, F. B. Wang and X. H. Xia, *J. Mater. Chem. A*,
125 2014, **2**, 9079-9084.

60. R. Z. Zhang and W. Chen, *Sci. Bull.*, 2015, **60**, 522-531.

61. R. Z. Zhang, S. J. He, Y. Z. Lu and W. Chen, *J. Mater. Chem. A*, 2015, **3**, 3559-3567.

62. Y. Xie, H. Q. Li, C. Z. Tang, S. S. Li, J. Li, Y. Lv, X. M. Wei and Y. J.
130 Song, *J. Mater. Chem. A*, 2014, **2**, 1631-1635.

63. H. T. Chung, J. H. Won and P. Zelenay, *Nat. commun.*, 2013, **4**, 1922.

64. G. Wu, M. Nelson, S. G. Ma, H. Meng, G. F. Cui and P. K. Shen, *Carbon*, 2011, **49**, 3972-3982.

65. W. Chen, L. Hong, A. L. Liu, J. Q. Liu, X. H. Lin and X. H. Xia,
135 *Talanta*, 2012, **99**, 643-648.

Three-dimensional Fe- and N-incorporated carbon structures as peroxidase mimics for fluorescent detection of hydrogen peroxide and glucose

Ruizhong Zhang, [a, b] Shuijian He, [a, b] Chunmei Zhang [a, b] and Wei Chen[*, a]
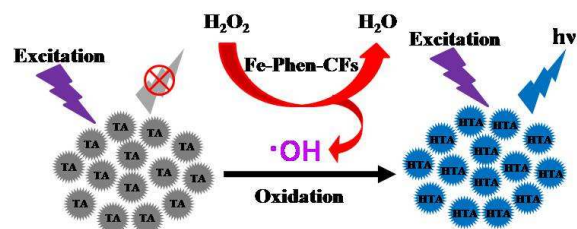
3D Fe- and N-incorporated carbon structure is synthesized as peroxidase mimics for fluorescent detection of hydrogen peroxide and glucose